Structural, mechanical, and electronic properties of defect-patterned graphene nanomeshes from first principles

H. Şahin[1] and S. Ciraci[1,2,*]

[1]*UNAM-Institute of Materials Science and Nanotechnology, Bilkent University, 06800 Ankara, Turkey*
[2]*Department of Physics, Bilkent University, 06800 Ankara, Turkey*

Motivated by the state of the art method for fabricating high-density periodic nanoscale defects in graphene, the structural, mechanical, and electronic properties of defect-patterned graphene nanomeshes including diverse morphologies of adatoms and holes are investigated by means of first-principles calculations within density functional theory. It is found that various patterns of adatom groups yield metallic or semimetallic, even semiconducting, behavior and specific patterns can be in a magnetic state. Even though the patterns of single adatoms dramatically alter the electronic structure of graphene, adatom groups of specific symmetry can maintain the Dirac fermion behavior. Nanoholes forming nanomesh are also investigated. Depending on the interplay between the repeat periodicity and the geometry of the hole, the nanomesh can be in different states ranging from metallic to semiconducting including semimetallic states with the bands crossing linearly at the Fermi level. We showed that forming periodically repeating superstructures in a graphene matrix can develop a promising technique for engineering nanomaterials with desired electronic and magnetic properties.

PACS number(s): 81.05.ue, 73.22.Pr, 63.22.Rc, 61.48.Gh

I. INTRODUCTION

Propagation of electron waves through a honeycomb lattice confers exceptional features to graphene.[1] Conduction of electrons within a one-atom-thick layer with minute scattering makes observation of quantum effects possible even at room temperature.[2,3] Experimental investigations have reported the observation of a half-integer quantum Hall effect for carriers in graphene and possible magnetoelectronic device applications.[4] Most of the unique properties of graphene are related to its monolayer lattice structure, linearly crossed π bands at the Fermi level with electron-hole symmetry. Recently, we showed that the honeycomb structure with linear band crossings at Dirac points is also common to Si and Ge.[5,6]

In an effort to make semimetallic graphene suitable for electronic applications, it has been functionalized to generate band gaps. It was theoretically shown that it is possible to induce band-gap opening produced by the adsorption of atomic hydrogen on graphene by choosing a specific adsorption periodicity.[7] It was also experimentally shown that B- and N-doped graphenes can be synthesized to exhibit p- and n-type semiconducting properties that can be systematically tuned with the dopant concentration.[8] The effect of hydrogenation and transition metal atom adsorption on the transport properties of graphene was also investigated theoretically.[9,10] Using symmetry arguments and tight binding calculations, it was shown that the periodic structure of defects (such as B and N impurities) on graphene can exhibit semimetallic and semiconductor behavior.[11] Moreover, a weak perturbation potential forming a large hexagonal lattice in a two-dimensional (2D) electron gas was shown to lead to a massless Dirac fermion Hamiltonian with linearly crossing bands at Dirac points.[12–14]

The majority of the current studies on graphene is devoted to its chemical modification to create derivatives with different structures and properties. So far three known derivatives of graphene have been successfully achieved in chemical reactions: graphene oxide (GO),[15–18] graphane (CH),[19–22] and, recently, fluorographene (CF).[23–25] Although GO is a wide-band-gap material that is important for device applications, its atomic structure, wherein the carbon atoms are decorated with epoxides, alcohols, and carboxylic acid groups, is not suitable for nanoscale manipulations. CH, obtained by exposing a carbon honeycomb structure to hydrogen plasma, is another example of a graphene-based chemical derivative. Upon hydrogenation, semimetallic graphene is converted into an insulator. CF, the 2D counterpart of Teflon, is the most recent focus of graphene research.

Much recently, the fabrication of large graphene sheets having a high-density array of nanoscale holes, called graphene nanomeshes (GNMs),[26] has been the landmark in controlling electronic properties at the nanoscale. Additionally, the formation of one-dimensional periodic Stone-Wales-type defects producing metallic nanowires on a graphene matrix has also been reported.[27] These recent advances have made the mesh configuration a controllable parameter for monitoring physical properties of nanostructures.[26–28] Earlier, interesting effects of periodically repeating holes on the electronic and mechanical properties of graphene nanoribbons were predicted from first-principles calculations.[29]

In this paper, we apply a supercell method to reveal the electronic, magnetic, and mechanical properties of graphene, which is patterned by various adsorbates or holes. The atomic structure of all adsorbates and holes are obtained after extensive structure optimization. These periodically repeating superstructures or nanomeshes display properties which are rather different from those of graphene. We showed that not all patterns of adsorbates or holes with a 2D hexagonal lattice on graphene have linear band crossing—only those which have specific rotation symmetries. However, depending on the size of patterns or holes and the repeat periodicity, a GNM can be in different states, ranging from semiconducting to semimetallic (with linear band crossings at the Fermi level).

II. COMPUTATIONAL METHODOLOGY

The present study revealed crucial effects of the point-group symmetry of nanomesh on the resulting properties. Here, we start with a brief discussion of hexagonal symmetry and apply a simple tight-binding model of π orbitals to reveal the effect of lattice symmetry on the band crossing.[30,31] Graphene has the space group $P6/mmm$ and the point-group symmetry D_{6h}. At the Γ point, the group of the wave vector is isomorphic to the point group D_{6h}.[32] However, irreducible representation of the wave-vector point group turns into D_{2h} and D_{3h} at high symmetry points M and K (or K'), respectively. It was shown that the tight-binding Hamiltonian with nearest-neighbor hopping parameter, $t = 2.7$ eV,

$$H = \sum_i \epsilon_i c_i^\dagger c_i + t \sum_{i,j} (c_i^\dagger c_j + \text{H.c.}), \qquad (1)$$

well approximates the π bands of perfect graphene.[30,31] Here $c_i^\dagger$ (c_i) is the creation (annihilation) operator of a π electron at lattice site i. The first term is the on-site energy of each carbon atom and equals the energy of the $2p_z$ orbital. Energy eigenvalues of graphene and another two hypothetical crystals having square and hexagonal lattices with a single atom in the cell are calculated, and contour plots of their energy band gaps in the Brillouin zone (BZ) are shown in Fig. 1. For graphene, the energy dispersion is linear in the vicinity of the K symmetry (Dirac) points, and the Fermi velocity, which is linearly dependent on the nearest-neighbor interaction parameter, can be given by the expression $v_F = 3td/2\hbar$.[33]

A hypothetical square lattice has a semimetallic band structure as shown in Fig. 1(b). In the reciprocal space the band gap is closed along the boundaries of squares. However, differing from graphene, these bands do not have a linear dispersion. A structure having a hexagonal lattice with a single π orbital per unit cell is shown in Fig. 1(c). Such a structure, having a single π orbital in each unit cell, may also be realized by adatom saturation of one type (A or B) of the carbon atoms of graphene. In this case, the structure has threefold rotation symmetry and hence six nearest neighbors. In this case, while saturation yields a dramatic change in the electronic structure,
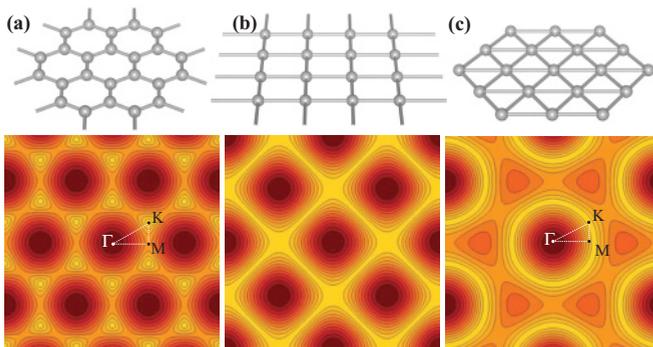

FIG. 1. (Color online) Contour plots for band gap. (a) Perfect graphene. (b) A crystal having a square lattice with a single atom in the unit cell. (c) A crystal having a hexagonal lattice with a single atom in the unit cell. Band crossing occurs along the yellow (light) contours on which the band gap becomes 0. The band gap takes its maximum value at the brown (dark) contours.

linear band crossings at the Fermi level still occur at points on a circle of radius $R = \frac{4\pi}{3\sqrt{3}}$ in BZ. As shown in Fig. 1(c), this circle passes through the corners of the hexagonal BZ of graphene. The Fermi velocity is calculated to be of the order of 10^6 m/s in the vicinity of band crossing points.

While the tight-binding model allowed us to understand the general features of the band gap in different lattices, it fails to account for the reconstruction and rebonding near the defect. In the rest of the paper we perform calculations from the first principles to investigate various types of defects. To this end we carried out spin-polarized plane-wave calculations[34,35] using the local density approximation (LDA)[36] and projector augmented wave (PAW)[37] potential. Patterns of defects are treated using supercell geometry, where a minimum of 10-Å vacuum spacing is kept between the adjacent graphene layers. The kinetic energy cutoff is determined after extensive convergence analysis. For the plane-wave basis set, the kinetic energy cutoff is taken to be $\hbar^2|\mathbf{k} + \mathbf{G}|^2/2m = 500$ eV. For partial occupancies the Methfessel-Paxton smearing method[38] is used. The convergence criterion of self-consistent field calculations is 10^{-5} eV for the total energy values. Using the conjugate gradient method, all atomic positions and sizes of unit cells were optimized until the atomic forces were less than 0.05 eV/Å. Pressures on the lattice unit cell were decreased to values less than 1 kB.

III. ADATOM PATTERNED GRAPHENE NANOMESHES

In this section we show how a periodic decoration of graphene by adatoms modifies the electronic structure. Here we considered H, F, O, and Mn adatoms, which are adsorbed at different sites and form (4×4) supercells on a graphene host matrix as shown in Figs. 2(a)–2(d). We did not consider interstitial or substitutional decoration, since experimental studies treating various foreign atoms, such as N,[8] O,[15] H,[19] F,[23] C,[39] Co,[40] Fe and Gd,[41] and Au and Pt,[42] revealed that these atoms prefer to be adsorbed at various sites on the surface of graphene, but none of them is adsorbed at interstitial sites or is substituted for a carbon atom.

Owing to the unpaired electron, a single hydrogen adatom adsorbed to a (4×4) supercell has a spin-polarized, semiconducting ground state with a net magnetic moment of $\mu = 1 \mu_B$. Upon adsorption of a hydrogen atom, the band structure of graphene changes dramatically. Instead of linear crossing of π and π^* bands at the Fermi level, dispersionless impurity bands occur, with a 0.1-eV indirect band gap. Similarly to hydrogen atoms, the most favorable adsorption site for a F atom on graphene is the top site of carbon atoms. Upon the adsorption of a F atom, sp^2 bondings of three C-C bonds below the F atom are dehybridized and form four tetrahedrally coordinated sp^3-type bondings. Differing from the decoration of H adatom, ground state is nonmagnetic and as a result of odd number of electrons F decorated graphene becomes metalized as shown in Fig. 2(b). The band crossing at the K points does not occur, since F adsorbed at the top of a C atom changes the sixfold rotation symmetry to the threefold rotation symmetry.

An oxygen atom favors the bridge site between two underlying C atoms. Upon the adsorption of an oxygen at the bridge site, two underlying C atoms become buckled by 0.36 Å. C-C and C-O bonds are calculated to be 1.51 and
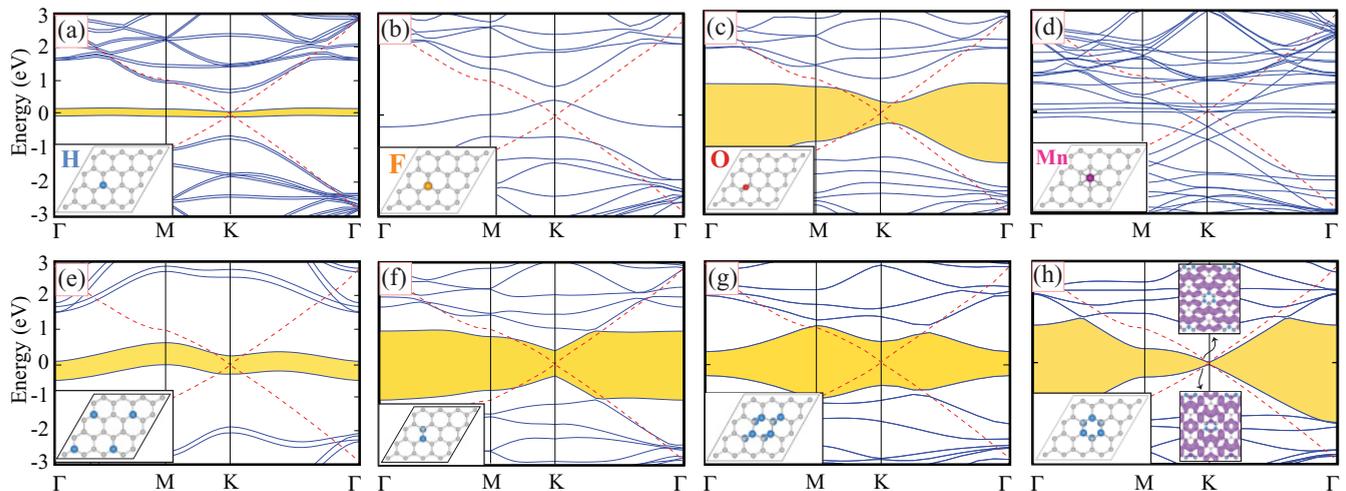
FIG. 2. (Color online) Spin-polarized energy band structure of periodic patterns consisting of (4×4) supercells, each having a single (a) hydrogen, (b) fluorine, (c) oxygen, and (d) manganese adatom. (e) A similar hydrogen pattern forming a (2×2) supercell on a graphene host matrix allowing significant coupling between adatoms. (f–h) Periodic patterns of two, eight, and six hydrogen atoms in a (4×4) graphene supercell, respectively. Insets: Isosurface of charge density of bands crossing near the K point. For comparison, linearly crossing π and π^* bands of a perfect graphene host matrix are also superimposed on the band structures. Zero energy is set at the Fermi level E_F. Band gaps are shaded yellow. All bands presented in the BZ corresponding to the (4×4) supercell.

1.44 Å, respectively. The resulting structure is a nonmagnetic semiconductor with a 0.63-eV direct band gap [Fig. 2(c)]. Valence and conduction band edges occur between the K and the Γ points. The adatom at the bridge site breaks the sixfold rotation symmetry and hence hinders the linear band crossing.

The situation is different in the case of Mn, which is adsorbed above the center of a hexagon in a graphene matrix and induces negligible deformation. Only the six nearest C atoms rise to a slightly higher (0.02 Å) position relative to the plane. Localized, nonbonding Mn-$3d$ orbitals form flat bands near the Fermi level. Besides, the sixfold rotation symmetry is maintained even after a Mn atom is adsorbed at the hollow site above the center of the hexagon. Accordingly, the metallic structure with a net magnetic moment of 3 μ_B per cell allows linear crossing of graphene bands at the K points in Fig. 2(d).

Having discussed the effect of periodic decoration by single adatoms, we next consider the periodic patterns of adatom groups. In Fig. 2(e) we show an electronic band structure corresponding to a relatively denser hydrogen coverage (C : H = 8). Such a nanomesh created by one-sided decoration of four hydrogen atoms in a (4×4) supercell gives rise to relatively dispersive bands and a net magnetic moment of 4 μ_B per supercell. Since the sixfold rotation symmetry of graphene is broken by adsorbed H atoms, linear crossing of bands does not occur. In a decoration involving two sides of graphene, two adjacent C atoms of different sublattices are saturated from different sides as shown in Fig. 2(f). Since equal numbers of A- and B-sublattice atoms are saturated, the structure is a nonmagnetic semiconductor with a band gap of 0.8 eV. Another pattern derived from a CH-like domain consisting of eight H atoms in Fig. 2(g) results in a band gap of 0.7 eV at the Γ point but a larger gap of 1 eV at the K point. This nanomesh presents an electronic structure rather different from that of both graphene and CH. The electronic structure is, however, different for a pattern of six H atoms, which saturate six carbon

atoms at the corner of a hexagon alternatingly from different sites: that is, three of them adsorbed to the A sublattice from one side and the remaining three adsorbed to the B sublattice from the other side. Even though the sixfold rotation symmetry has changed to S_6 symmetry, both point-group symmetries allow linear band crossing as shown in Fig. 2(h). This case demonstrates the crucial role played by the intrinsic symmetry of the pattern in determining the electronic structure.[11–13]

Let us now take a closer look at the triangular patterns of adatom groups that have hexagonal symmetry. In Fig. 3, we plot these π and π^* bands in the vicinity ($\Delta k = 0.03$ Å^{-1}) of the K-symmetry point for different patterns on supercells of different sizes, that is, (4×4) and (8×8) (C_{128} and C_{32}) supercells. H_6 and H_{12} patterns, which have 0.06- and 0.09-eV band gaps at the K point, indicate that the band gap opening increases with increasing pattern size, hence increasing coupling. In the (8×8) supercell the interaction between periodically repeating H_6 patterns is hindered, and hence linear crossing of π and π^* bands at the K-symmetry
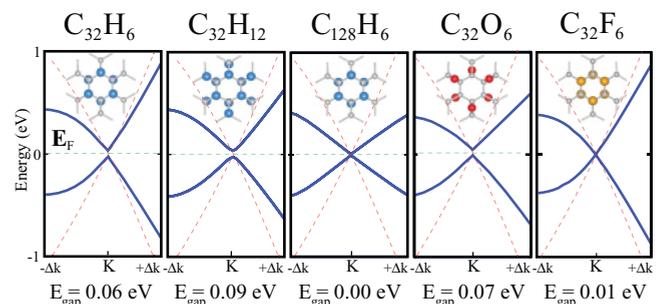

FIG. 3. (Color online) Band structures showing the effects of coupling between various patterns as a function of their size and the mesh size (supercell). Linearly crossing π and π^* bands of graphene are shown by dashed (red) lines.

point similar to that in bare graphene is attained. By expressing these bands as $\mathbf{k} = \mathbf{K} + \mathbf{q}$ and neglecting the second-order terms with respect to q^2, the dispersion of the energy bands can be given as $E(\mathbf{q}) \simeq \mathbf{v_F}\hbar|\mathbf{q}|$. Here the Fermi velocity v_F is calculated as 0.7×10^6 m/s (i.e., ~ 0.6 of the Fermi velocity calculated for Dirac fermions in perfect graphene).

We also present an example of an O_6 pattern analogous to H_{12} decoration of a (4×4) supercell ($C_{32}H_{12}$) of graphene in Fig. 3. In this pattern three O atoms are bound alternatingly to the bridge site at one site, and the remaining three atoms, to another site. Here it is seen that denser O patterns are not favored due to strong O-O repulsion. Linear crossing of bands at the K point can also be achieved by O adatoms forming a periodically repeating O_6 pattern. The small band gap in Fig. 3 can be closed if the supercell size is increased, to hinder coupling between them. This example implies that patterns similar to that obtained using H atoms can be created by the passivation of p-orbital electrons with O atoms. In the case of fluorination of (4×4) graphene by F_6 decoration, similarly to H_6, linear π and π^* bands gets closer with a very small (0.01-eV) band gap at the K point. Finally, the isosurface charge densities of these linearly crossing bands near the K point indicates that they mainly originate from graphene π orbitals, with a small amount of mixing from the adatom [see Fig. 2(h)].

IV. HOLE-PATTERNED GRAPHENE NANOMESHES

Similarly to adatom patterns on graphene, nanomeshes generated from holes periodically patterned on a graphene matrix also exhibit interesting features. This conclusion, drawn from theoretical calculations, is in line with the findings obtained from the fabrication of GNMs by means of the block-copolymer-assisted nanopatterning process. It has been shown that GNMs having a high-density periodic array of holes display promising advantages relative to existing graphene devices.[26,27] Thanks to the advances in the preparation of high-quality nanoscale hard masks[26,27,43] under laboratory conditions, theoretical studies in this field become more relevant for applications. Here we carry out calculations for holes with a 1- to 2-nm repeat period and a 2- to 10-Å diameter. In Fig. 4(a) we describe the geometric parameters of C_n hole defects forming a hexagonal lattice, where n denotes the number of C atoms removed from the graphene matrix to make a hole. For nanoholes, we define the hole size as the maximum diameter of the C_n hole defective region. After the creation of a C_1 defect (i.e., single C vacancy), Jahn-Teller-type distortion changes the positions of the surrounding C atoms slightly. The resulting structure attains a net magnetic moment of 1 μ_B. The origin of magnetism in defective graphene sheets and the character of electronic states induced by the vacancy resulting in flat bands around the Fermi level have been investigated in some recent studies.[44–46] Upon the removal of C atoms ($n > 1$), graphene is reconstructed to result in a significant modification of the atomic configuration around the hole. For example, after relaxation of the atomic structure, the C_2 defective region becomes an octagon-shaped hole surrounded by two pentagons and six hexagons. Similarly, as a result of Stone-Wales-type transformation, each C_4 defect region also turns into a nonagon-shaped hole. As reported
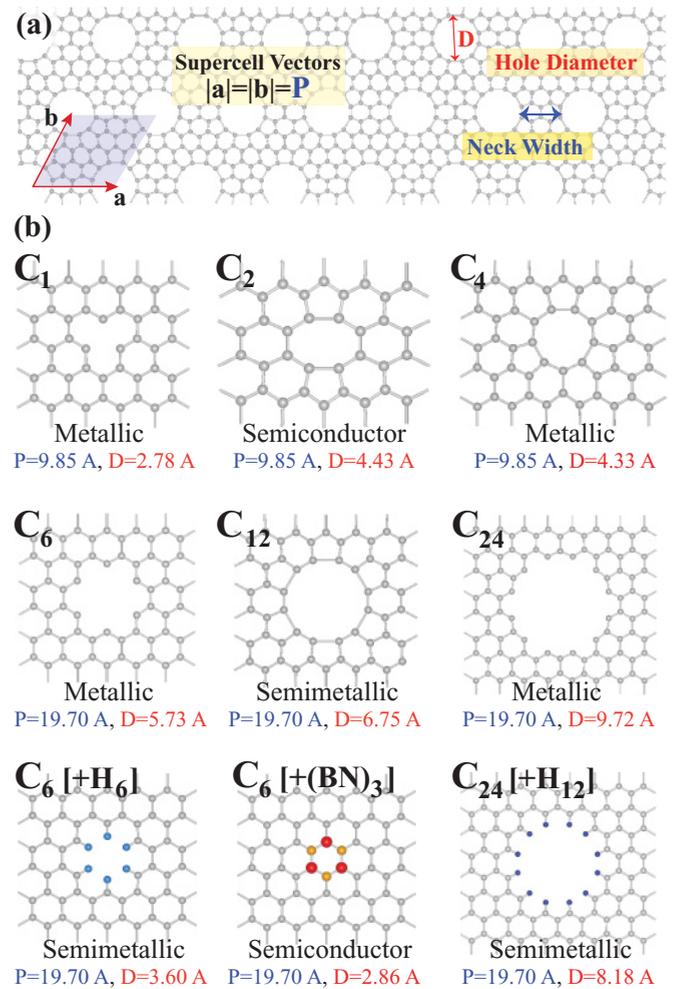

FIG. 4. (Color online) (a) Structural parameters for the nanomesh of a C_n hole. (b) Large supercells of a hexagonal lattice, each containing a single hole of C_1, C_2, C_4, C_6, C_{12}, and C_{24}. Nanomeshes in the third row were obtained by saturating C_6 and C_{24} holes with hydrogen and, also, with alternating B and N atoms.

experimentally,[47] a hole region is surrounded by pentagonal and hexagonal rings of C atoms to keep the flatness of the sheet. While the honeycomb lattice symmetry of the graphene matrix does not change considerably for larger defects, C_6 and C_{24}, the hole region of C_{12} takes an almost-circular shape surrounded by regular pentagons and hexagons. Apparently, the trend in the shape of the hole region is determined by whether the edges of the domain are zigzag or armchair shaped.

The energy band structures of GNMs exhibit interesting variations with respect to their sizes, diameters, and nanohole shapes as illustrated in Fig. 4(b). While nanomeshes of the C_1 defect show metallic behavior, the periodic structure of the C_2 defect becomes an indirect band gap semiconductor of 0.65 eV. However, π and π^* bands above the Fermi level are still very close to each other (0.09-eV gap) at the K point. The C_4 defective GNM shows metallic behavior. The situation becomes even more remarkable for larger defects: C_6, C_{12}, and C_{24}. GNMs including either a C_6 or a C_{24} hole have zigzag edges and are metals with an antiferromagnetic ground state. We note that defect-induced flat electronic bands around the Fermi level occur if the electron spins become unpaired.
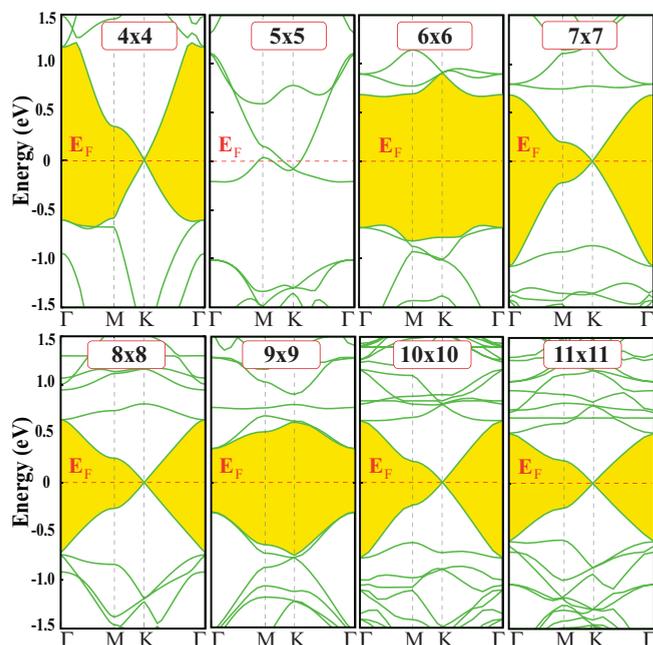
FIG. 5. (Color online) Band structure of nanomeshes of C_{12} forming in $(n \times n)$ supercells of graphene, with $n = 4 \ldots 11$.

FIG. 6. (Color online) (a–c) Rectangular patterns of C_{12} holes repeated in (3×6), (4×8), and (5×10) graphene supercells. Insets: Atomic structures of nanomeshes. (d) Semimetallic electronic structure and isosurface charge densities of valence (V) and conduction (C) bands of (5×10) nanomesh are also shown.

Besides, the reconstruction or the dimerization of dangling carbon bonds around the defect can cause the flat bands in the gap to disappear. Interestingly, nanomeshes of C_6 and C_{24} holes, which are metallic, become semimetal upon the saturation of dangling bonds of carbon atoms around the hole with hydrogen atoms. This metal-semimetal transformation can have applications in graphene-based nanoelectronics. On the other hand, GNM of C_6 turns semiconducting with a band gap of 0.1 eV upon the termination of the dangling bonds of C atoms around the hole by B and N alternatingly to from a B_3N_3 hexagon. The band opening is explained by the breaking of sixfold symmetry due to B_3N_3 hexagon. The formation extended B_nN_n honeycomb structure can be achieved directly in the course of epitaxial growth of graphene and single layer BN.[48,49]

As for a GNM with C_{12}, it is a nonmagnetic semimetal because the carbon atoms at the edge are dimerized. Analysis of the orbital character of linearly crossing π and π^* bands near the K point using isosurface charge densities suggests that these bands originate from bonding and antibonding combinations of π orbitals at the neck and around the C_6 hole. Here we discuss an important aspect of GNMs with C_{12}: that the size of the hexagonal supercell or repeat periodicity of C_{12} is crucial for the resulting electronic structure. Figure 5 shows band structures of GNMs including a single C_{12} hole in an $(n \times n)$ supercell where $n = 4 \ldots 11$. For $n = 4$, the GNM has a neck region consisting of a single hexagon and is a semimetal. For $n = 5$, the GNM is a metal and has a neck region which is relatively thicker but its C-C bond angles deviate strongly from $120°$. Surprisingly, a GNM with $n = 6$ is a semiconductor having a 1.3- eV band gap. The bond angles continue to deviate from those of graphene. However, above $n = 7$ the bond angles in the neck region start to be graphene-like, with a regular honeycomb structure. GNMs with both $n = 7$ and $n = 8$ are semimetals and have π and π^*
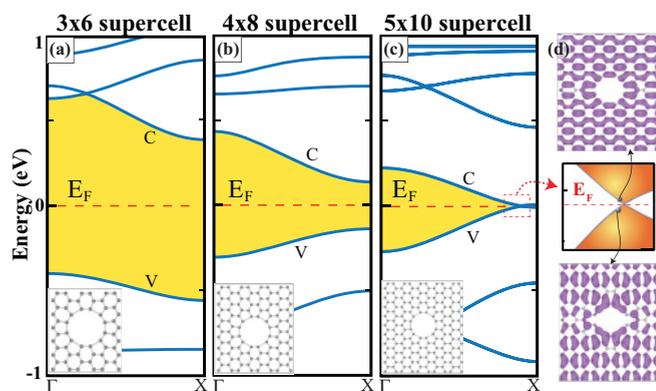
bands which cross linearly at the Fermi level at the K point. The isosurface charge densities of these bands near K points demonstrate that they, in fact, originate from the combination of graphene π orbitals. As n increases, GNMs exhibit a similar trend for $n = 6–9$; namely, they are semiconductors for $n = 9$ but semimetals for $n = 10$ and 11. This variation of band gaps is reminiscent of the family behavior of graphene nanoribbons and is related to the variation in the thickness of necks between periodically repeating C_{12} holes.[29,50] Here, even if the sixfold rotation symmetry is conserved, the band gap opens for every $n = 3 \times N$, with N being an integer $\geqslant 2$. However, this gap becomes smaller and eventually is closed as $n \rightarrow \infty$. We also note that the family behavior of GNMs is related to the edge structure of the hole. With regard to the size of the GNM of C_{12}, we also note that the lattice constants of the corresponding $(n \times n)$ supercell are modified with size. For example, for $n = 11$, the lattice constant of the supercell is contracted by 1%, the contraction is 4% for $n = 5$ and 40% for $n = 4$.

Finally, in addition to triangular defect patterns, we also discuss the electronic structure of holes arranged in a rectangular lattice. In Fig. 6 we show the electronic band structures of C_{12} nanomeshes realized by (3×6), (4×8), and (5×10) supercells. While C_{12} holes in small rectangular supercells with a low-repeat periodicity (leading to significant coupling) become semiconducting, a semimetallic nature indigenous to that of graphene is achieved in large supercells. As shown in Fig. 6(c), even if the rotation symmetry required for band crossing is absent, graphene-like Bloch wave functions in the rectangular mesh of sparse patterns of C_{12} holes show a semimetallic behavior. This indicates that as the size of the supercell increases and the neck gets wider relative to the size of the hole, the symmetry requirement necessary for linear band crossing can be relaxed.

V. MECHANICAL PROPERTIES OF NANOMESHES

A honeycomb structure with sp^2 bonding underlies the unusual mechanical properties providing a very high in-plane strength but transversal flexibility. Here we investigate how the mechanical properties of nanomeshes are generated with patterns of adatoms or holes. We focus on the harmonic range

of the elastic deformation, where the structure responds to strain ϵ linearly. Here ϵ is the elongation per unit length. The strain energy is defined as $E_s = E_T(\epsilon) - E_T(\epsilon = 0)$; namely, the total energy at a given strain ϵ minus the total energy at zero strain. Normally, the Young's modulus is the value which characterizes the mechanical strength of a bulk material. Owing to ambiguities in defining the Young's modulus of 2D structures like a GNM, one can use the in-plane stiffness $C = (1/A_0)(\partial^2 E_S/\partial \epsilon^2)$ in terms of the equilibrium area of the supercell, A_0.[51,52] We calculate the in-plane stiffness of graphene, and nanomeshes consisting of $C_{32}H_6$, BN-substituted graphene (i.e., $C_{26}[(BN)_3]$, and a C_6 hole in graphene using a (4×4) supercell in Fig. 3. The stiffness of bare graphene is calculated to be 334 N/m, which is in good agreement with the experimental value of 340 ± 50 N/m. Furthermore, the in-plane stiffness values of nanomeshes generated on graphene through B_3N_3 substitution, an H_6 adatom pattern, and a C_6 hole are 308, 283, and 167 N/m, respectively. Apparently, the bare graphene matrix is weakened by the formation of any of these nanomeshes. In addition to the calculation of in-plane stiffness, we extend our analysis to include the plastic deformation region, where the honeycomb-like structure is destroyed after the yielding point (i.e., the onset of plastic deformation), and the GNM undergoes a massive structural deformation. Our preliminary simulations indicate that the yielding strain of a C_6-hole GNM is significantly lower than the yielding strains of both $C_{26}[(BN)_3]$ and $C_{32}H_6$ GNMs.

VI. CONCLUSIONS

While graphene and its various derivatives, GO, CH, and CF, are important nanomaterials with diverse electronic, magnetic, and mechanical properties, their properties can be modified and multiplied using different methods of functionalization. The most pronounced property of graphene, namely, linearly crossing bands at the Fermi level, and the electron-hole symmetry arising therefrom, is usually destroyed when graphene is functionalized through dopant or vacancy defects. In this work we have demonstrated that the electron-hole symmetry, even Dirac fermion behavior, can be recovered for periodically repeating superstructures or nanomeshes having special point-group symmetry. In this study we have considered nanomeshes, which are generated by decoration of adatoms, adatom groups, or holes which repeats periodically in a graphene matrix. We found that the types of adatoms and their patterns, the geometry of the holes of carbon atoms, and the sizes and lattice symmetries of nanomesh provide us with several parameters with which to engineer the electronic and magnetic properties of nanomeshes. In particular, we have shown that by varying only the size of the nanomesh including a specific hole, one can tune between metallic and semiconducting states including semimetal with linearly crossing bands. This is reminiscent of the family behavior of graphene nanoribbons.

*Corresponding author. ciraci@fen.bilkent.edu.tr

[1] A. K. Geim and K. S. Novoselov, Nat. Mater. **6**, 183 (2007).

[2] X. Wang, Y. Ouyang, X. Li, H. Wang, J. Guo, and H. Dai, Phys. Rev. Lett. **100**, 206803 (2008).

[3] C. Berger, Z. Song, T. Li, X. Li, A. Y. Ogbazghi, R. Feng, Z. Dai, A. N. Marchenkov, E. H. Conrad, P. N. First, and W. A. de Heer, Science **312**, 1191 (2006).

[4] Y. Zhang, Yan-Wen Tan, H. L. Stormer, and P. Kim, Nature (London) **438**, 201 (2005).

[5] S. Cahangirov, M. Topsakal, E. Akturk, H. Şahin, and S. Ciraci, Phys. Rev. Lett. **102**, 236804 (2009).

[6] H. Şahin, S. Cahangirov, M. Topsakal, E. Bekaroglu, E. Aktürk, R. T. Senger, and S. Ciraci, Phys. Rev. B **80**, 155453 (2009).

[7] J. M. Garcia-Lastra, Phys. Rev. B **82**, 235418 (2010).

[8] L. S. Panchakarla, K. S. Subrahmanyam, S. K. Saha, A. Govindaraj, H. R. Krishnamurthy, U. V. Waghmare, and C. N. R. Rao, Adv. Mater. **21**, 4726 (2009).

[9] H. Şahin and R. T. Senger, Phys. Rev. B **78**, 205423 (2008).

[10] H. Şahin, R. T. Senger, and S. Ciraci, J. Appl. Phys. **108**, 074301 (2010).

[11] R. Martinazzo, S. Casolo, and G. F. Tantardini, Phys. Rev. B **81**, 245420 (2010).

[12] R. P. Tiwari and D. Stroud, Phys. Rev. B **79**, 205435 (2009).

[13] C. -H. Park and S. G. Louie, Nano Lett. **9**, 1793 (2009).

[14] M. Gibertini, A. Singha, V. Pellegrini, M. Polini, G. Vignale, A. Pinczuk, L. N. Pfeiffer, and K. W. West, Phys. Rev. B **79**, 241406 (2009).

[15] D. A. Dikin, S. Stankovich, E. J. Zimney, R. D. Piner, G. H. B. Dommett, G. Evmenenko, S. T. Nguyen, and R. S. Ruoff, Nature (London) **448**, 457 (2007).

[16] S. Stankovich, R. D. Piner, X. Chen, N. Wu, S. T. Nguyen, and R. S. Ruoff, J. Mater. Chem. **16**, 155 (2006).

[17] G. Eda, G. Fanchini, and M. Chhowalla, Nature Nanotechnol. **3**, 270 (2008).

[18] C. Gomez-Navarro, R. T. Weitz, A. M. Bittner, M. Scolari, A. Mews, M. Burghard, and K. Kern, Nano Lett. **7**, 3499 (2007).

[19] D. C. Elias, R. R. Nair, T. M. G. Mohiuddin, S. V. Morozov, P. Blake, M. P. Halsall, A. C. Ferrari, D. W. Boukhvalov, M. I. Katsnelson *et al.*, Science **323**, 610 (2009).

[20] J. O. Sofo, A. S. Chaudhari, and G. D. Barber, Phys. Rev. B **75**, 153401 (2007).

[21] H. Şahin, C. Ataca, and S. Ciraci, Appl. Phys. Lett. **95**, 222510 (2009).

[22]M. Z. S. Flores, P. A. S. Autreto, S. B. Legoas, and D. S. Galvao, Nanotechnology **20**, 465704 (2009).

[23]R. R. Nair, W. Ren, R. Jalil, I. Riaz, V. G. Kravets, L. Britnell, P. Blake, F. Schedin, A. S. Mayorov, S. Yuan *et al.*, Small **6**, 2877 (2010).

[24]S.-H. Cheng, K. Zou, F. Okino, H. R. Gutierrez, A. Gupta, N. Shen, P. C. Eklund, J. O. Sofo, and J. Zhu, Phys. Rev. B **81**, 205435 (2010).

[25]H. Şahin, M. Topsakal, and S. Ciraci, Phys. Rev. B **83**, 115432 (2011).

[26]J. Bai, X. Zhong, S. Jiang, Y. Huang, and X. Duan, Nature Nanotech. **5**, 190 (2010).

[27]J. Lahiri, Y. Lin, P. Bozkurt, I. I. Oleynik, and M. Batzill, Nature Nanotech. **5**, 326 (2010).

[28]R. Balog, B. Jorgensen, L. Nilsson, M. Andersen, E. Rienks, M. Bianchi, M. Fanetti, E. Lagsgaard, A. Baraldi, S. Lizzit *et al.*, Nat. Mater. **9**, 315 (2010).

[29]M. Topsakal, E. Akturk, H. Sevincli, and S. Ciraci, Phys. Rev. B **78**, 235435 (2008).

[30]P. R. Wallace, Phys. Rev. **71**, 622 (1947).

[31]C. Bena and G. Montambaux, New J. Phys. **11**, 095003 (2009).

[32]L. M. Malard, M. A. Pimenta, G. Dresselhaus, and M. S. Dresselhaus, Phys. Rep. **473**, 51 (2009).

[33]A. H. Castro Neto, F. Guinea, N. M. R. Peres, K. S. Novoselov, and A. K. Geim, Rev. Mod. Phys. **81**, 109 (2009).

[34]G. Kresse and J. Hafner, Phys. Rev. B **47**, 558 (1993).

[35]G. Kresse and J. Furthmüller, Phys. Rev. B **54**, 11169 (1996).

[36]D. M. Ceperley and B. J. Alder, Phys. Rev. Lett. **45**, 566 (1980).

[37]P. E. Blochl, Phys. Rev. B **50**, 17953 (1994).

[38]M. Methfessel and A. T. Paxton, Phys. Rev. B **40**, 3616 (1989).

[39]A. Hashimoto, K. Suenaga, A. Gloter, K. Urita, and S. Iijima, Nature **430**, 870 (2004).

[40]V. W. Brar, R. Decker, Hans-Michael Solowan, Y. Wang, L. Maserati, K. T. Chan, H. Lee, C. O. Girit, A. Zettl, S. G. Louie *et al.*, Nature Phys. **7**, 43 (2011).

[41]M. Hupalo, S. Binz, and M. C. Tringides, J. Phys. Condens. Matter **23**, 045005 (2011).

[42]Y. Gan, L. Sun, and F. Banhart, Small **4**, 587 (2008).

[43]L. Zhang, S. Diao, Y. Nie, K. Yan, N. Liu, B. Dai, Q. Xie, A. Reina, J. Kong, and Z. Liu, J. Am. Chem. Soc. (in press).

[44]E. H. Lieb, Phys. Rev. Lett. **62**, 1201 (1989).

[45]O. V. Yazyev and L. Helm, Phys. Rev. B **75**, 125408 (2007).

[46]B. R. K. Nanda, M. Sherafati, Z. Popovic, and S. Satpathy, e-print arXiv:1105.1129.

[47]A. Hashimoto, K. Suenaga, A. Gloter, K. Urita, and S. Iijima, Nature (London) **430**, 870 (2004).

[48]S. Cahangirov and S. Ciraci, Phys. Rev. B **83**, 165448 (2011).

[49]L. Ci, L. Song, C. Jin, D. Jariwala, D. Wu, Y. Li, A. Srivastava, Z. F. Wang, K. Storr, L. Balicas *et al.*, Nat. Mater. **9**, 430 (2010).

[50]S. Cahangirov, M. Topsakal, and S. Ciraci, Phys. Rev. B **81**, 195120 (2010).

[51]B. I. Yakobson, C. J. Brabec, and J. Bernholc, Phys. Rev. Lett. **76**, 2511 (1996).

[52]C. D. Reddy, S. Rajendran, and K. M. Liew, Nanotechnology **17**, 864 (2006).